Alterations of hepatic energy metabolism in murine models of obesity, diabetes and fatty liver diseases

Bedair Dewidar,[a,b] Lucia Mastrototaro,[a,b] Cornelia Englisch,[a,b] Claudia Ress,[c,d] Cesare Granata,[a,b] Elisabeth Rohbeck,[a,b] Dominik Pesta,[a,b] Geronimo Heilmann,[a,b] Martin Wolkersdorfer,[e] Irene Esposito,[f] Michelle Reina Do Fundo,[a,b] Fariba Zivehe,[a,b] Aslihan Yavas,[f] and Michael Roden[a,b,g,*]

[a]Institute for Clinical Diabetology, German Diabetes Center, Leibniz Center for Diabetes Research at Heinrich-Heine-University Düsseldorf, Düsseldorf, Germany
[b]German Center for Diabetes Research, Partner Düsseldorf, München-Neuherberg, Germany
[c]Department of Internal Medicine I, Medical University Innsbruck, Innsbruck, Austria
[d]Christian Doppler Laboratory for Insulin Resistance, Department of Internal Medicine I, Medical University Innsbruck, Innsbruck, Austria
[e]Landesapotheke Salzburg, Department of Production, Hospital Pharmacy, Salzburg, Austria
[f]Institute of Pathology, Heinrich-Heine-University Düsseldorf, Düsseldorf, Germany
[g]Department of Endocrinology and Diabetology, Medical Faculty and University Hospital Düsseldorf, Heinrich-Heine-University Düsseldorf, Düsseldorf, Germany

Summary

Background Disturbed hepatic energy metabolism contributes to non-alcoholic fatty liver (NAFLD), but the development of changes over time and obesity- or diabetes-related mechanisms remained unclear.

Methods Two-day old male C57BL/6j mice received streptozotocin (STZ) or placebo (PLC) and then high-fat (HFD) or regular chow diet (RCD) from week 4 (W4) to either W8 or W16, yielding control [CTRL = PLC + RCD], diabetes [DIAB = STZ + RCD], obesity [OBES = PLC + HFD] and diabetes-related non-alcoholic steatohepatitis [NASH = STZ + HFD] models. Mitochondrial respiration was measured by high-resolution respirometry and insulin-sensitive glucose metabolism by hyperinsulinemic-euglycemic clamps with stable isotope dilution.

Findings NASH showed higher steatosis and NAFLD activity already at W8 and liver fibrosis at W16 (all p < 0.01 vs CTRL). Ballooning was increased in DIAB and NASH at W16 (p < 0.01 vs CTRL). At W16, insulin sensitivity was 47%, 58% and 75% lower in DIAB, NASH and OBES (p < 0.001 vs CTRL). Hepatic uncoupled fatty acid oxidation (FAO)-associated respiration was reduced in OBES at W8, but doubled in DIAB and NASH at W16 (p < 0.01 vs CTRL) and correlated with biomarkers of unfolded protein response (UPR), oxidative stress and hepatic expression of certain enzymes (acetyl-CoA carboxylase 2, *Acc2*; carnitine palmitoyltransferase I, *Cpt1a*). Tricarboxylic acid cycle (TCA)-driven respiration was lower in OBES at W8 and doubled in DIAB at W16 (p < 0.0001 vs CTRL), which positively correlated with expression of genes related to lipolysis.

Interpretation Hepatic mitochondria adapt to various metabolic challenges with increasing FAO-driven respiration, which is linked to dysfunctional UPR, systemic oxidative stress, insulin resistance and altered lipid metabolism. In a diabetes model, higher TCA-linked respiration reflected mitochondrial adaptation to greater hepatic lipid turnover.

Funding Funding bodies that contributed to this study were listed in the acknowledgements section.

Keywords: Fatty liver; Type 2 diabetes; Insulin resistance; Type 1 diabetes; Mitochondria; High-resolution respirometry; Unfolded protein response

Introduction

Non-alcoholic fatty liver disease (NAFLD) describes abnormalities, ranging from steatosis, non-alcoholic steatohepatitis (NASH) and fibrosis to hepatocellular carcinoma, which are rapidly increasing worldwide.[1,2] Specifically, obesity and type 2 diabetes mellitus

---

Research in context

Evidence before this study
Non-alcoholic fatty liver disease (NAFLD) is tightly associated with obesity and type 2 diabetes mellitus (T2DM). Conflicting results have been reported for hepatic mitochondrial functionality in humans with obesity, T2DM or NAFLD. Hepatic oxidative capacity can be unchanged or increased in obese NAFLD and T2DM, but decreased in steatohepatitis (NASH). Some studies showed reduced mitochondrial respiration in NASH with higher fibrosis scores, while others reported mitochondrial respiration to be independent of NAFLD severity. Finally, type 1 diabetes (T1DM) may also feature altered hepatic energy homeostasis.

Added value of this study
This study investigated hepatic mitochondrial respiration by high-resolution respirometry in murine models of obesity, diabetes without or with NASH and control mice during the early course of metabolic liver disease. This design allowed to evaluate time-dependent changes in mitochondrial respiration, but also to separate the effect of diabetes and obesity from that of NAFLD. Furthermore, mechanisms possibly affecting mitochondrial respiration such as insulin sensitivity, lipid metabolism, mitochondrial biogenesis and oxidative and endoplasmic reticulum (ER) stress were investigated.

Implications of all the available evidence
Specifically, hepatic mitochondrial oxidation is upregulated during the development of diet-induced obesity and diabetes with or without NASH. This confirms hepatic mitochondrial plasticity, which has been suggested from the few available human cross-sectional studies. Hepatic mitochondrial plasticity is operative along with altered tissue-specific insulin sensitivity and lipid metabolism, systemic oxidative stress and importantly also with hepatic ER stress.

(T2DM) are tightly and mutually associated with NAFLD and its progression.[3,4]

Mitochondria are responsible for oxidative phosphorylation (OXPHOS) and adenosine triphosphate (ATP) synthesis, but also for generating reactive oxygen species (ROS) and specific cellular functions.[5] Conflicting results have been reported for hepatic mitochondrial functionality in humans with obesity, T2DM or NAFLD.[5–7] Using stable isotope methods, hepatic mitochondrial oxidation was found to be doubled[8] or unchanged in NAFLD.[9] Using high-resolution respirometry (HRR), hepatic oxidative capacity was up to 5-fold higher in obese people with or without steatosis when compared to lean humans,[10] but unchanged in T2DM and even decreased in NASH.[10,11] In line, overweight/obese persons with NASH showed impaired activity of mitochondrial complexes,[12] rate-limiting enzymes of fatty acid oxidation (FAO)[13] and ATP recovery upon fructose[14] as well as mitochondrial structural abnormalities.[15] Likewise, people with NASH and higher fibrosis scores showed reduced mitochondrial respiration,[16] while others reported mitochondrial respiration to be independent of NAFLD severity in obese persons.[17] These different results might reflect disease heterogeneity, as recently demonstrated by the identification of diabetes subtypes including severe insulin deficient to severe insulin resistant diabetes with specific risks for diabetes-related complications, such as NAFLD.[18] Altered hepatic energy homeostasis may be also present in individuals with short- and long-standing T1DM, as shown by lower hepatic ATP content.[19–21] Although these findings suggest that adaptation to obesity- and diabetes-related metabolic challenges, allowing for meeting the bioenergetic needs (termed mitochondrial plasticity), is lost with disease progression,[6,7,10] comprehensive information on the different features of hepatic energy metabolism are scarce.

As the association of obesity and NAFLD with diabetes makes it difficult to separate the different metabolic effects and their impact on hepatic mitochondrial function, we aimed to monitor possible hepatic alterations during the development of obesity, diabetes and NAFLD in specific mouse models, which allows to overcome ethical and methodological limitations for such experiments in humans. Thus, this study compared hepatic mitochondrial respiration by HRR in murine models of obesity (OBES), diabetes (DIAB), diabetes with NASH (NASH) and control mice (CTRL) during the early course of metabolic liver disease, at 8 (W8) and 16 weeks (W16). Furthermore, this study investigated mechanisms possibly affecting mitochondrial function, i.e. tissue-specific insulin sensitivity, lipid metabolism, mitochondrial biogenesis, oxidative and endoplasmic reticulum (ER) stress.

Methods
Study design
This study was performed to compare alterations in hepatic mitochondrial respiration in murine models for diabetes (DIAB), obesity (OBES), diabetes-related non-alcoholic steatohepatitis (NASH) and healthy control (CTRL) using parallel group design. A priori Sample size was calculated based on maximal uncoupled respiration from preliminary data from diet-induced NASH model using G*power software (HHU, Düsseldorf, Germany) with a cut-off of p < 0.05 (error type 2 (β) is adjusted to 0.2 and power to 80%). Two different respiratory protocols was investigated at two different

time-points i.e. 8 (W8) and 16 weeks (W16). The investigators carried out the animal experiments were not blinded to the groups. All mice used in the study were age-matched and exclusively male, because of their higher susceptibility to develop advanced stages of NAFLD as compared to female mice.[22]

Animal models

Mice were maintained on a 12-h light-dark cycle in standard cages with free access to the respective diets and water. To examine diabetes-related NASH, NASH was generated by using the Stelic Animal Model (STAM).[22] Briefly, two-day old male C57BL/6J mice received a single subcutaneous dose of 200 μg streptozotocin (STZ)/mouse (Sigma-Aldrich, Taufkirchen, Germany), which induces partial β-cell damage,[22] or with citrate vehicle (placebo, PLC) (Fig. 1a). Four weeks after injection (W4), mice were fed either high-fat diet (HFD) (60% of calories from fat, 20% from protein, and 20% carbohydrate, #D12492, Research Diets Inc., New Jersey, USA) or continued their regular chow diet (RCD) (10% of calories from fat, 23% from protein and 67% from carbohydrate, #V1537-000, ssniff Spezialdiäten GmbH, Soest, Germany).

This design yielded four groups: (i) CTRL [PLC + RCD], (ii) DIAB [STZ + RCD], (iii) OBES [PLC + HFD] and (iv) NASH [STZ + HFD]. All mice underwent weekly monitoring of blood glucose (Accu-Check, Roche, Mannheim, Germany), body weight and food consumption and monthly monitoring of lean and fat mass by quantitative nuclear magnetic resonance imaging (Whole Body Composition Analyzer; EchoMRI, Houston, TX, USA). The study was terminated if mice showed more than 20% reduction in body weight or elevated blood glucose (>500–600 mg/dl) for more than three consecutive measurements. To avoid acute effects of clamp-induced hyperinsulinemia, one cohort was used only for measurement of mitochondrial respiration using high-resolution respirometry (HRR) and other analyses at W8 and W16, whereas the other cohort was used exclusively for assessing insulin sensitivity using hyperinsulinemic-euglycemic clamps at W16. For HRR, liver and soleus muscle tissues were harvested from the sacrificed mice and immediately transferred to ice-cold preservation medium (BIOPS solution)[23] until HRR in permeabilized tissue within 2 h. An aliquot of 100 mg liver was rapidly frozen in O.C.T medium (Sakura Finetek GmbH, Umkirch, Germany) for Oil red O staining, while another aliquot of 100 mg was fixed in 4% paraformaldehyde and embedded in paraffin for histological examination. The remaining liver tissue was rapidly snap-frozen and stored in liquid nitrogen for further molecular analyses. Trunk blood was collected in the fed state for plasma analyses.

Hyperinsulinemic-euglycemic clamp (HEC)

HEC was performed in a separate cohort of mice as described before.[24] In Brief, a silicon catheter (Instech,
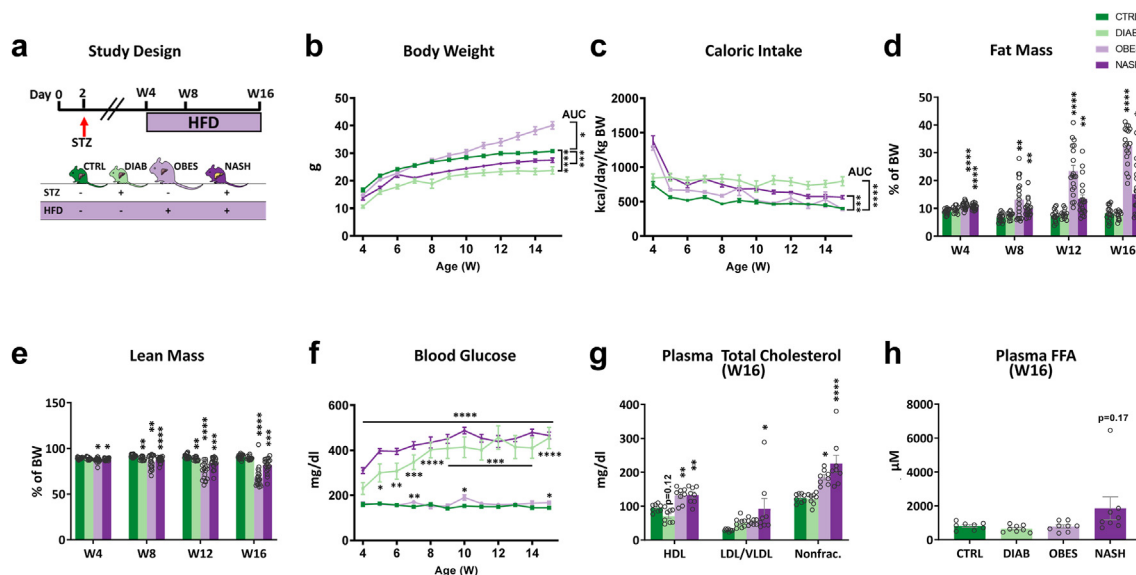

Fig. 1: Metabolic features of the animal models. (a) Study design and mice groups. Weekly changes in (b) body weight (BW) and (c) relative caloric intake. Area under the curve (AUC) was compared between the groups with 1-way ANOVA. (d) Relative fat mass and (e) lean mass determined by MRI. (f) Weekly changes in blood glucose. Plasma levels of (g) total cholesterol and (h) free fatty acids (FFA) at week 16 (W16). Mean ± SEM, n = 8–18/group, (d and e) analysed with 2-way ANOVA (1-factor: mouse group, 2-factor: time), (f) with repeated-measure ANOVA, (g) with 2-way ANOVA (1-factor: mouse group, 2-factor: cholesterol fraction), and (h) with 1-way ANOVA. *p < 0.05; **p < 0.01; ***p < 0.001; ****p < 0.0001 vs CTRL.

Pennsylvania, USA) was placed into the right jugular vein of 15W-old mice under isoflurane (Abbott GmbH, Wiesbaden, Germany) anesthesia. After recovery and acclimatization (3–5 days), mice were fasted for 6 h before starting HEC. To assess basal whole-body glucose turnover, D-[6,6-^{2}H$_2$]glucose (≥98% enriched, Cambridge Isotope Laboratories, Andover, MA, USA) was infused at a rate of 0.18 mg/kg/min for 120 min. HEC started with a priming dose (40 mU/kg/min for 10 min) of human regular insulin (Sanofi-Aventis, Frankfurt, Germany) and continued with insulin infusion at a constant rate of 8 mU/kg/min. Blood glucose concentrations were checked every 5 min by Accu-Check (Roche, Mannheim, Germany) and maintained at 120 ± 10 mg/dl by periodically adjusting a 20% glucose infusion (B. Braun GmbH, Glandorf, Germany). D-[6,6-^{2}H$_2$]glucose was infused together with insulin solution (0.14 mg/kg/min) and also with 20% glucose solution, containing 1.6 mg/ml D-[6,6-^{2}H$_2$]glucose, to obtain stable tracer concentrations during varying glucose infusion rates.[24] Blood samples for measuring D-[6,6-^{2}H$_2$]glucose enrichments were taken every 10 min during the last 30 min of the basal period as well as HEC. For enrichment analysis, plasma was first deproteinized, D-[6,6-^{2}H$_2$]glucose was then derivatized to aldonitrile-pentaacetate and quantified with gas-chromatography-mass spectrometry as previously described in humans with minor modifications due lower mice blood volume.[25] Blood (20 µl) was collected in EDTA-containing capillary tubes from the tail vein before and after HEC for measurement of blood glucose (Biovision, Milpitas, CA, USA) and insulin concentrations (insulin ELISA kit, Mercodia, Uppsala, Sweden) following the manufacturer's instruction. Glucose infusion rate (GIR, mg/kg/min) during the last 35 min of the clamp (steady-state) was used to assess whole-body insulin sensitivity. Whole-body insulin-mediated glucose disposal (R$_d$) was calculated by modified Steele's single pool steady-state equations.[26,27] The difference between R$_d$ and GIR yields the rate of endogenous glucose production (EGP). Hepatic insulin sensitivity is given as percentage of insulin-mediated suppression of EGP vs basal conditions, whereas whole-body insulin sensitivity is represented as clamp R$_d$ normalized to steady-state insulinemia.

Mitochondrial respiration

Mitochondrial respiration was assessed in duplicate in mechanically permeabilized liver as well as mechanically and saponin permeabilized soleus muscle, using two protocols per tissue in Oxygraph-2k chambers (Oroboros Instruments, Innsbruck, Austria) as described.[23]

The protocol for TCA-driven respiration included the following titrations: addition of 2 mM malate and 10 mM pyruvate, to determine leak respiration (L) with electron input through complex I (CI) in the absence of adenylates [PM]$_{LN}$; 2.5 mM ADP, to determine coupled respiration (P) with electron input through CI [PM]$_P$; 10 mM glutamate, to determine P with complete electron input through CI [PMG]$_P$; 10 mM succinate, to determine P with convergent electron input through CI and II [PMGS]$_P$; 6 µM cytochrome c, to check the integrity of outer mitochondrial membrane; 5 µM oligomycin, to determine L with convergent electron input through CI and II [PMGS]$_L$; stepwise titrations of carbonyl cyanide-p-trifluoromethoxyphenylhydrazone (FCCP, 0.5–1.25 µM), to determine electron transfer system capacity (E) with convergent electron input through CI and II [PMGS]$_E$; 5 µM antimycin A, to determine the residual oxygen consumption [ROX] (equivalent to non-mitochondrial respiration).

The protocol for FAO-linked respiration included the following titrations: addition of 2 mM malate and 1 mM octanoyl-carnitine, to determine L with electron input through electron-transferring flavoprotein (ETF) in the absence of adenylates [OctM]$_{LN}$; 2.5 mM ADP, to determine P with electron input through ETF [OctM]$_P$; 6 µM cytochrome c, to test outer mitochondrial membrane integrity; 5 µM oligomycin, to determine L with electron input through ETF [OctM]$_L$; titration of FCCP (0.5–1.25 µM), to determine E with electron input through ETF [OctM]$_E$; 5 µM antimycin A, to determine ROX. Samples presenting a greater than 15% increase in respiration following cytochrome c addition were excluded.[28] To account for changes in mitochondrial content, we determined mitochondria (mt-)specific respiration, obtained by normalizing respiration values to maximal citrate synthase activity (CSA) as a biomarker of mitochondrial content.[29] CSA was assessed spectrophotometrically using the Citrate Synthase Assay kit (Sigma-Aldrich). Respiratory flux control ratios (FCRs) were calculated: the inverse respiratory control ratio (RCR$_{inv}$) is the quotient between [PMGS]$_{L/P}$ (TCA protocol) and [OctM]$_{L/P}$ (FAO protocol); the leak control ratio (LCR) is the quotient between [PMGS]$_{L/E}$ (TCA protocol) and [OctM]$_{L/E}$ (FAO protocol).[23]

Biomarkers related to oxidative stress

Liver and kidney thiobarbituric acid reactive substances (TBARS) were measured fluorometrically (Cell Biolabs, San Diego, CA, USA). Liver catalase activity (Cayman, Michigan, USA), superoxide dismutase (SOD) activity, and the ratio of reduced and oxidized glutathione (GSH/GSSG) were measured colorimetrically in tissue lysates. Liver and plasma 8-hydroxy-2′-deoxyguanosine (8-OHdG) as well as plasma advanced glycation end products (AGE) were measured by ELISA (Cell Biolabs). RedoxSYSTM (Luoxis Diagnostics, Inc., Englewood, CO, USA) was used to assess systemic oxidative stress from plasma static oxidation-reduction potential (ORP) and antioxidant capacity as described.[30]

Histology

Paraffin-embedded liver sections were first deparaffinized in xylene, rehydrated in serial dilutions of ethanol, and then stained by hematoxylin and eosin (H&E) and special stains for iron (Prussian blue), collagen (Masson's trichrome), or glycogen (Diastase pre-treated Periodic acid-Schiff) for evaluation of NAFLD histological scores (e.g. steatosis, hepatocellular ballooning, lobular inflammation, and fibrosis grade) by an expert liver pathologist, blinded to the protocol.[31] The NAFLD activity score (NAS) was calculated by summation of individual scores for steatosis (0–3), lobular inflammation (0–3), and hepatocellular ballooning (0–2).[32] In addition, Liver collagen level and liver steatosis were evaluated in 16W-old mice by Sirius red[33] and Oil red O staining,[34] respectively. Percentage of Sirius red and Oil red O positive stained area was calculated as the mean from 10 non-overlapping 10-fold magnified fields using QuPath (Version 0.2.3, Belfast, UK) and ImageJ Softwares (Version 1.53, Maryland, USA) as previously described.[35,36]

Immunohistochemistry

Immunohistochemistry was performed as previously described.[37] Briefly, liver tissue sections (5 μm) were deparaffinized in xylene and rehydrated in serial dilutions of ethanol. After deparaffinization, antigen retrieval was performed at boiling temperature in citrate buffer (10 mM, pH 6.0) for 20 min for CD45 or in presence of proteinase K (Dako, Jena, Germany) for 5 min at room temperature (RT) for F4/80 antigen. Slides were incubated with endogenous peroxidase blocker (Dako) for 20 min at RT, followed by blocking of endogenous biotin (Abcam, Cambridge, UK). Next, sections were incubated with primary antibodies at 4 °C overnight (Supplementary Table S2). On the next day, slides were washed with phosphate-buffered saline (PBS) for 5 min and incubated with secondary antibodies for 1 h at RT (Supplementary Table S3). Brown color staining was developed with diaminobenzidine (DAB; Sigma-Aldrich) and nuclei were counterstained with hematoxylin (Sigma-Aldrich). Stained slides were scanned by a VS200 slide scanner (Olympus, Tokyo, Japan). Percentage of positive stained area was calculated as described before. Liver tissues incubated with PBS instead of primary antibody served as negative control.

Immunoblotting

Proteins were extracted from approximately 30 mg of liver tissue and homogenized in 300 μl of lysis buffer (25 mM trisaminomethane-hydrochloride (Tris-HCl), pH 7.4, 150 mM NaCl, 0.20% Nonidet P-40, 1 mM ethylenediaminetetraacetic acid (EDTA), and 0.1% sodium dodecyl sulfate (SDS)) supplemented with a Protease Inhibitor Cocktail and the Phosphatase Inhibitor Cocktail II (Roche). Extracted proteins were diluted with reducing Laemmli sample buffer containing 2-mercaptoethanol (Biorad, Hercules, CA, USA), boiled 5 min at 95 °C and loaded onto SDS polyacrylamide gradient gels (4–20% Mini-PROTEAN® TGX™ Precast Protein Gels, Biorad). An inter-run calibrator (IRC) was loaded to each gel to account for between-run differences. After electrophoresis, proteins were transferred to a polyvinylidene difluoride (PVDF) membrane (Merck Millipore, Darmstadt, Germany) using the Trans-Blot Turbo System (Bio-Rad, Munich, Germany). The PVDF membrane was blocked with 5% non-fat milk in Tris-buffered saline with Tween 20 (TBST buffer: 10 mM Tris, pH 8.0, 150 mM NaCl, and 0.5% Tween 20) for 2 h at RT. Afterwards, the membranes were incubated overnight with primary antibodies at 4 °C (Supplementary Table S2). Next day, membranes were washed with TBST buffer and incubated with horseradish peroxidase (HRP)-conjugated secondary antibodies for 1 h at RT (Supplementary Table S3). Finally, membranes were coated with Immobilon Western Chemiluminescent HRP Substrate (Merck Millipore) and proteins were detected using a ChemiDoc imaging system in combination with the software ImageLab 6.0.1 (Biorad) for densitometric analysis. Finally, data were normalized either to GAPDH as reference loading control or to total protein content. Phosphorylated proteins were additionally normalized to total protein content of non-phosphorylated form.

Quantitative real-time-PCR (RT-PCR)

Total RNA was isolated from 20 mg of frozen liver using the RNeasy Mini Kit (Qiagen, Düsseldorf, Germany) and from 30 to 50 mg of frozen subcutaneous and epididymal white adipose tissue using the QIAzol Lysis Reagent (Qiagen, Cat. No. 79306). cDNA was transcribed from 1000 ng total RNA with the QuantiTect Reverse Transcription Kit (Qiagen, Cat. No. 205311) and used for RT-PCR with QuantiTect SYBR® Green PCR Kit (Qiagen, Cat. No. 204145) in a StepOnePlus RT-PCR System (Applied Biosystems, Waltham, MA, USA) using QuantiTect Primer Assays (Qiagen) and self-designed primers (Eurofins, Ebersberg, Germany). The primers are listed in Supplementary Table S4. Ct values were first normalized to geometric mean of Ct of the 3 reference genes i.e. *Ppia*, *B2m*, and *Hprt1* (for liver) or *Ppia*, *18SRNA* and *Ywhaz* (for adipose tissues), then to Ct of IRC to obtain the expression fold change following the ΔΔCt method.[38] A melting curve was created to ensure primer specificity. Each sample was measured in triplicate.

Analysis of further biomarkers

Blood samples were centrifuged at 3000*g* for 10 min at 4 °C. Plasma was stored in new reaction tubes at –80 °C. Circulating concentrations of FFA were measured using the FFA Assay Kit (Cell Biolabs). Total cholesterol was measured colorimetrically in LDL/VLDL and HDL

fractions after cleavage of cholesterol ester by cholesterol esterase using HDL and LDL/VLDL Cholesterol Assay Kit (Cell Biolabs). Total non-fractionated cholesterol was calculated by summation of total cholesterol in both LDL/VLDL and HDF fractions.

Hepatic triglyceride concentration was measured using Triglyceride Quantification Colorimetric/Fluorometric Kit (Biovision). Liver contents of collagen 1α1 (Cusabio, Houston, TX, USA), tumor necrosis factor-alpha (TNF-α) (Abnova, Taipei, Taiwan) and monocyte chemoattractant protein 1 (MCP-1) (Thermo Fischer Scientific, Waltham, MA, USA) and plasma levels of pro-collagen CIII (pro-CIII) (Cusabio) were analyzed by ELISA according to the manufacturer's instructions. Liver hydroxyproline was quantified spectrophotometrically (Cell Biolabs) as a proxy of liver total collagen content.

Ethics
All experiments were performed according to the guidelines of the society for laboratory animal science (GV-SOLAS) upon approval by regulatory authorities (License Nr. 84-02.04.2017.A253, LANUV, NRW, Germany).

Statistics
Data were analyzed using GraphPad Prism (Version 9, La Jolla, CA, USA) and expressed as mean ± standard error of the mean (SEM). Continuous data were statistically analyzed using 1-way or 2-way ANOVA, followed by Tukey's multiple comparison test. The normal distribution of key parameters of this study was confirmed using Shapiro–Wilk test or Kolmogorov–Smirnov test. Ordinal scoring data were represented as median plus intra-quantile range and analyzed by Kruskal–Wallis test, followed by Dunn's comparison test. Dichotomous categorical outcome (tumor presence) was analyzed by Fisher's exact test. Changes in blood glucose over time was analyzed using repeated-measure ANOVA. Association between variables was calculated using Pearson correlation and visualized using R package "Corrplot". p-values <0.05 were considered to indicate statistically significant differences.

Role of funders
The funding source of this study played no role in the study design, data collection, analysis, interpretation, writing, or editing of the manuscript.

Results
Development of metabolic alterations
As compared to CRTL, body weight increase was lower in DIAB and NASH starting from W5, but higher in OBES starting from W11 (Fig. 1b). Caloric intake was higher in NASH and DIAB (area under the curve; AUC: p < 0.001 and p < 0.0001, respectively, one-way ANOVA) (Fig. 1c). Starting from W4, relative body fat mass was higher in OBES and NASH than in CTRL (Fig. 1d). Weights of brown (BAT), epididymal white (EWAT), and subcutaneous white adipose tissue (SWAT) were higher in OBES (W8, W16), whereas only EWAT was higher in NASH than in CTRL (W16) (Supplementary Fig. S1a). Relative lean body mass started to be lower in OBES and NASH at W4, but was reduced in all three groups at W8 and W12 vs CTRL (Fig. 1e). Similar changes were observed for skeletal muscle weights (Supplementary Fig. S1b).

By design, DIAB and NASH showed excessive hyperglycemia (p < 0.001 vs OBES and CTRL, repeated-measure ANOVA), whereas OBES showed only moderate hyperglycemia (W7, W10, W15) than CTRL (Fig. 1f). Only in NASH, plasma low density (LDL)- and very low-density lipoprotein (VLDL)-cholesterol were higher at W16 (p < 0.05, two-way ANOVA) (Fig. 1g) and plasma FFA tended to be higher (p = 0.17, one-way ANOVA) vs CTRL (Fig. 1h).

Collectively, NASH features comparable hyperglycemia as DIAB, but also higher body fat mass and dyslipidemia as OBES, despite no body weight increase.

Development of NAFLD
Already at W8, median NAFLD activity score (NAS) was increased in NASH, mainly due to higher steatosis (p < 0.001, Kruskal–Wallis test) and lobular inflammation, whereas histological NAFLD scores did not differ among DIAB, OBES, and CTRL. At W16, median NAS remained elevated in NASH and also increased to 2.50 in DIAB, mainly due to steatosis and hepatocellular ballooning in NASH and hepatocellular ballooning in DIAB (Table 1). Dysplastic hepatocellular nodules were found in 45% of NASH and 50% of DIAB at W16 (p < 0.05 vs CTRL, Fischer's exact test, data not shown).

At W16, liver triacylglycerol content from ELISA was 2.8- and 4.2-fold higher in both OBES and NASH, respectively (p < 0.05 and p < 0.0001 vs CTRL, one-way ANOVA), whereas steatosis from Oil red O staining was 23-fold higher in NASH only (p < 0.0001 vs CTRL, one-way ANOVA). Relative liver weight was elevated in the three groups at W16 as compared to CTRL (Fig. 2a–c). At the same time, histopathological analysis showed an elevated liver fibrosis score (Table 1) and liver collagen content from Sirius red staining was 2.9-fold higher in NASH, which associated with increased plasma pro-collagen CIII (PCIII) levels (Fig. 2a and d). In line, liver α-SMA protein content and total liver hydroxyproline, as a proxy of collagen, were significantly higher in NASH, whereas liver collagen 1α1 protein level was increased in NASH and OBES (Fig. 2d and Supplementary Fig. S2a). The mRNA levels of hepatic fibrogenesis-related genes either increased, e.g. tissue inhibitor of metalloproteinase 1 (Timp1) (p < 0.05, one-way ANOVA) (Supplementary Fig. S2a), tended to be higher, e.g. Collagen type 1α1 (Col1a1) (p = 0.08, one-way ANOVA) or did not change, e.g. transforming growth factor β

	CTRL	DIAB	OBES	NASH
W8				
n	8	8	15	12
NAS (0–8)	0.50 [0.00–1.75]	2.00 [1.00–2.00]	0.00 [0.00–1.00]	**4.00***** [3.25–4.75]
Steatosis score (0–3)	0.00 [0.00–0.00]	0.00 [0.00–0.00]	0.00 [0.00–0.00]	**1.00***** [1.00–1.00]
HC ballooning score (0–2)	0.00 [0.00–1.00]	1.00 [0.00–2.00]	0.00 [0.00–0.00]	1.50 [0.25–2.00]
Lobular inflam. score (0–3)	0.00 [0.00–0.75]	0.50 [0.00–1.00]	0.00 [0.00–0.00]	**1.00**** [1.00–2.00]
Fibrosis grade (0–4)	0.00 [0.00–0.00]	0.00 [0.00–0.00]	0.00 [0.00–0.00]	0.00 [0.00–0.00]
W16				
n	11	10	11	11
NAS (0–8)	1.00 [0.00–1.00]	**2.50*** [1.00–4.00]	1.00 [1.00–2.00]	**4.00***** [3.00–4.00]
Steatosis score (0–3)	0.00 [0.00–0.00]	0.00 [0.00–0.00]	0.00 [0.00–0.00]	**1.00****** [1.00–1.00]
HC ballooning score (0–2)	1.00 [0.00–1.00]	**2.00**** [1.00–2.00]	1.00 [0.00–1.00]	**2.00***** [1.00–2.00]
Lobular inflam. score (0–3)	0.00 [0.00–1.00]	1.00 [0.00–1.25]	0.00 [0.00–1.00]	1.00 [0.00–1.00]
Fibrosis grade (0–4)	0.00 [0.00–0.00]	0.00 [0.00–0.25]	0.00 [0.00–0.00]	**1.00**** [0.00–2.00]

Data were represented as median plus [interquantile range]. Data were analysed by Kruskal–Wallis test, followed by Dunn's multiple comparisons test. NAS: NAFLD activity score calculated from summation of individual scores for steatosis, hepatocellular (HC) ballooning, and lobular inflammation. *p < 0.05; **p < 0.01; ***p < 0.001; ****p < 0.0001 vs CTRL. Significantly altered scores are highlighted in bold.

Table 1: Histopathological analysis of mice liver.

(*Tgfb1*) and alpha-smooth actin (*Acta2*) as compared to CTRL (data not shown). Hepatic TNF-α protein levels were 31%, 38%, and 67% higher in DIAB, OBES, and NASH; MCP-1 was 32% and 55% higher in DIAB and NASH, respectively, than in CTRL (Fig. 2e). Liver inflammatory F4/80$^+$ macrophages and CD45$^+$ monocytes as well as mRNA expression of hepatic cytokines and chemokines did not differ between groups (Supplementary Fig. S2b–S2d).

Taken together, NASH shows the highest NAS with steatosis, ballooning and fibrosis as well as pro-inflammatory cytokine expression.
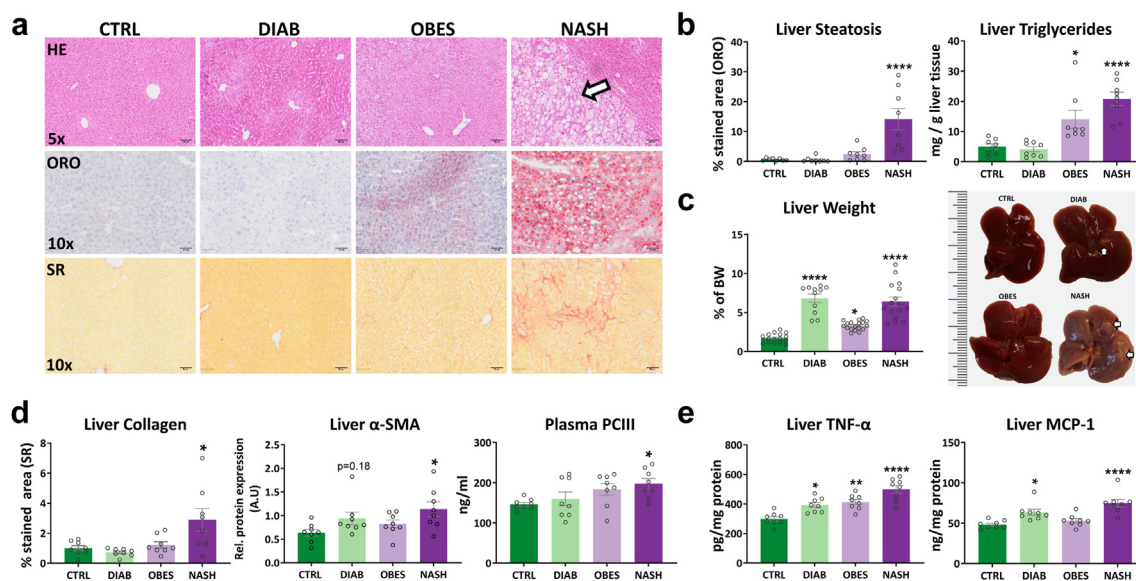

Fig. 2: **NASH development (W16).** (a) Representative pictures show hematoxylin and eosin (HE), Oil red O (ORO), and Sirius red (SR) staining. White arrow highlights area with hepatocellular carcinoma and steatosis. (b) Liver fat content from ORO staining and liver triglycerides. (c) Liver weight normalized to total body weight (BW). White arrows in liver macroscopic pictures highlight dysplastic liver nodules. (d) Liver fibrosis markers. (e) Hepatic protein level of inflammatory cytokine TNF-α and chemokine MCP-1. Scale bar 100 μm (top panels); 50 μm (middle and bottom panels). Mean ± SEM, n = 7–8/group (n for liver weight = 11–18/group), analysed with 1-way ANOVA. *p < 0.05; **p < 0.01; ****p < 0.0001 vs CTRL.

Tissue-specific insulin sensitivity

Hepatic and whole-body (skeletal muscle) insulin sensitivity were measured at W16 (Fig. 3a). Fasting blood glucose was 180% higher in DIAB and NASH than in CTRL (both $p < 0.0001$, two-way ANOVA). During clamp steady-state, blood glucose was comparable in all groups (Fig. 3b, Supplementary Fig. S3a), while plasma insulin was higher in OBES than in DIAB and NASH (Fig. 3c). Glucose infusion rate (GIR) was 50%, 54%, and 68% lower in OBES, DIAB, and NASH, respectively (all $p < 0.0001$ vs CTRL, one-way ANOVA) indicating whole-body insulin resistance (Fig. 3d, Supplementary Fig. S3b). Likewise, insulin-stimulated whole-body glucose disposal (R_d), normalized to steady-state insulinemia, was 47%, 58%, and 75% lower in DIAB, NASH, and OBES (all $p < 0.001$ vs CTRL, one-way ANOVA) confirming severe skeletal muscle insulin resistance (Fig. 3e). Basal endogenous glucose production (EGP) was higher only in DIAB (Supplementary Fig. S3c). Under hyperinsulinemic clamp conditions, insulin-mediated suppression of EGP did not differ across the groups (Supplementary Fig. S3d). However, it was lower in OBES ($p < 0.05$, one-way ANOVA) and tended to be lower in DIAB and NASH ($p < 0.30$, $p < 0.10$, respectively, vs CTRL, one-way ANOVA) upon normalization to steady-state insulinemia (Fig. 3f). Under physiological (fed, non-fasting) insulinemia, phosphorylation of hepatic AKT^{T308} and AKT^{S473} was decreased in NASH confirming hepatic insulin resistance at the molecular level (Fig. 3g).

Taken together, DIAB, NASH, and OBES exhibit major whole-body (skeletal muscle) insulin resistance, whereas hepatic insulin resistance is marginal in NASH and OBES under these experimental conditions.

Liver and skeletal muscle (m. soleus) respiration

TCA- and FAO-driven mitochondrial respiration was assessed in permeabilized liver and soleus muscle at W8 and W16 using two different respiratory protocols (Fig. 4a). Substrates for electron transfer complex (ETC) I, e.g. malate (M), pyruvate (P), glutamate (G), and ETC II, i.e. succinate (S) were applied in TCA protocol, whereas octanoyl-carnitine plus malate (OctM) were used in the FAO protocol.[39] Substrate-driven O_2 flux was measured in presence of adenylate (ADP) and oligomycin (OMY), to determine coupled (P) and leak respiration (L), respectively. Both protocols included titration of the uncoupler FCCP to determine ETC capacity [E].

In livers, mitochondrial (mt) content, as assessed from citrate synthase activity (CSA), was increased only in OBES at W8 ($p < 0.05$ vs CTRL, one-way ANOVA) (Fig. 4b and c). For mt-specific respiration, as assessed by normalization to CSA, NASH showed elevated $[OctM]_P$, whereas OBES had reduced $[OctM]_E$ and $[PMGS]_E$ at W8 (Fig. 4d and e). At W16, $[OctM]_P$, was approximately doubled in DIAB and NASH (both $p < 0.01$ vs CTRL, two-way ANOVA). Similar increases in $[OctM]_E$ were observed among all groups (Fig. 4f). Conversely, mt-specific $[PMGS]_P$ and $[PMGS]_E$ were doubled in DIAB only (Fig. 4g). Liver mass-specific respiration, i.e. O_2 fluxes normalized to liver weight, followed a similar pattern of mt-specific respiration (Supplementary Fig. S4a). Except for inverse respiratory
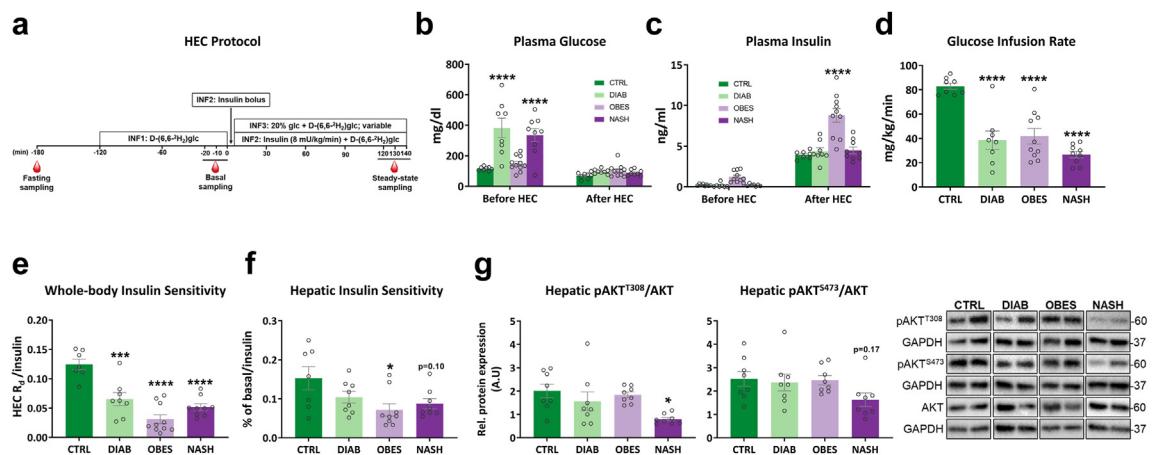

Fig. 3: Tissue-specific insulin sensitivity (W16). (a) Protocol for hyperinsulinemic-euglycemic clamp (HEC). (b) Fasting plasma glucose and (c) plasma insulin before and after HEC measured by ELISA. (d) Glucose infusion rate normalized to body weight. (e) Whole-body insulin sensitivity given as clamp R_d (mg/kg/min), normalized to steady-state insulinemia (pM). (f) Hepatic insulin sensitivity given as percentage of insulin-mediated suppression of EGP vs basal conditions (normalized to steady-state insulinemia). (g) Ratio of phosphorylated AKT (T308 and S473) to total AKT. Immunoblot shows two representative mice for each group based on densitometric quantification. Mean ± SEM, n = 7–11/group, (b and c) analysed with 2-way ANOVA (1-factor: mouse group, 2-factor: time), (d–g) with 1-way ANOVA. *$p < 0.05$; ***$p < 0.001$; ****$p < 0.0001$ vs CTRL.
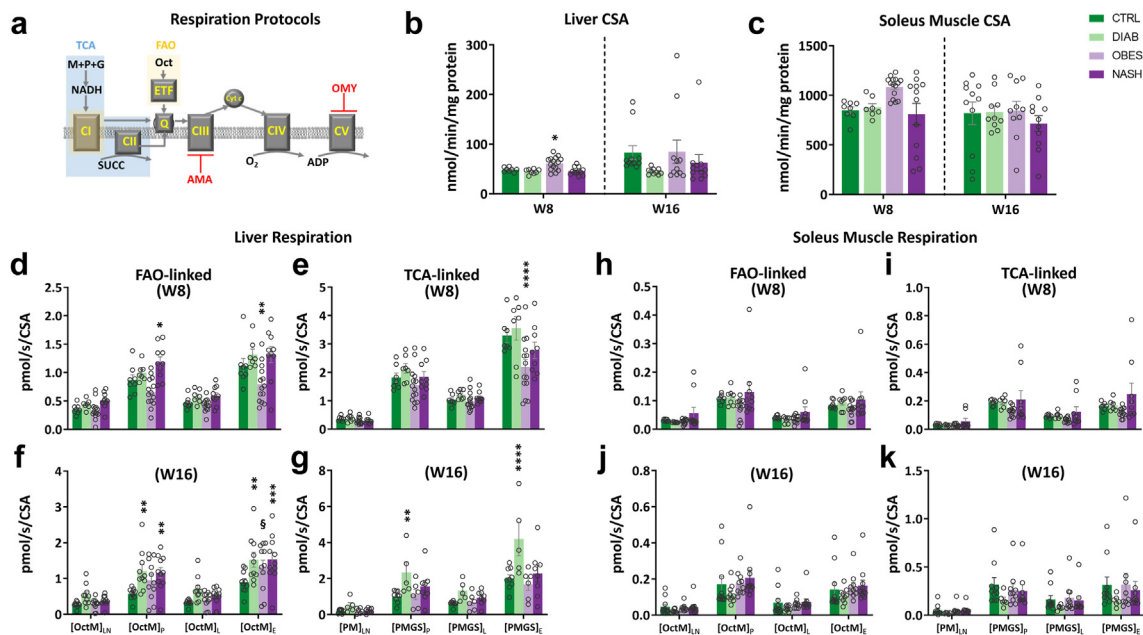
Fig. 4: Liver and skeletal muscle (m. soleus) mitochondria-specific respiration. (a) Substrate-uncoupler-inhibitor titration (SUIT) protocols, (b and c) citrate synthase activity (CSA), and (d–k) mt-specific FAO- and TCA-driven O_2 fluxes in permeabilized liver and soleus muscle at W8 and W16. Mean ± SEM, n = 5–15/group, (b and c) analysed with 1-way ANOVA, (d–k) with 2-way ANOVA (1-factor: mouse group, 2-factor: substrate). §p = 0.05, *p < 0.05; **p < 0.01; ***p < 0.001; ****p < 0.0001 vs CTRL. ETF: electron-transferring flavoprotein; P: pyruvate; M: malate; G: glutamate; S: succinate; Oct: octanoyl-carnitine. $_{LN}$: leak respiration with no adenylates; $_P$: coupled respiration; $_L$: leak respiration after addition of oligomycin; $_E$: electron transfer system capacity.

control ratio (RCR$_{inv}$) from FAO (decreased in 16W-old OBES) and leak control ratio (LCR) from TCA (elevated in 8W-old OBES and 16W-old NASH), hepatic respiratory flux control ratios (FCRs), i.e. RCR$_{inv}$ and LCR, were comparable among the groups at both time points (Supplementary Fig. S5).

In contrast to liver, no changes in mt-specific respiration (Fig. 4h–k) and FCRs (data not shown) were found in soleus muscle at W8 and W16. Muscle mass-specific respiration revealed reduced [PMGS]$_P$ in NASH at W8 and DIAB at W16 and increased [OctM]$_P$ and [OctM]$_E$ in NASH and OBES at W16 (Supplementary Fig. S4b).

Collectively, liver, but not soleus muscle mitochondria, adapt to metabolic challenges by increasing FAO-derived mitochondrial respiration in OBES and NASH, but by increasing both FAO- and TCA-derived respiration in DIAB.

Hepatic mitochondrial respiratory complexes, mitochondrial biogenesis and oxidative stress

To better understand the alterations in hepatic respiration, we measured the protein expression of ETC I–V and mRNA levels of mitochondrial biogenesis-related genes. At W16, only ETC V protein was significantly increased in OBES vs CTRL (Supplementary Fig. S6a and S6b) and positively correlated with overall hepatic mt-specific [OctM]$_P$ and [OctM]$_E$ (Pearson r = 0.63 and 0.69, respectively, both p < 0.001, correlation t-test). There were no differences in mRNA expression of mitochondrial biogenesis-related genes across all groups (Supplementary Fig. S6c).

Although altered mitochondrial respiration frequently associates with greater ROS production,[10,40] hepatic markers of oxidative stress (thiobarbituric acid reactive substances (TBARS), 8-hydroxy-2′-deoxyguanosine, 8-OHdG, nitrotyrosine) and antioxidative capacity (catalase, GSH/GSSG) were comparable between the groups (Fig. 5a, Supplementary Fig. S7a, nitrotyrosine data not shown). However, both DIAB and NASH featured impaired plasma antioxidant capacity with concomitant rise of oxidation-reduction potential (Fig. 5b), indicating greater systemic oxidative stress.[30] DIAB showed also higher plasma 8-OHdG than CTRL (Supplementary Fig. S7b). Systemic antioxidant capacity was indeed negatively correlated with overall hepatic mt-specific [OctM]$_P$, [OctM]$_E$ and [PMGS]$_P$ (Pearson r = −0.39, −0.39, and −0.48; all p < 0.05, correlation t-test). In line, hepatic superoxide dismutase (SOD) activity was reduced by 31%, 52%, 75% in DIAB, OBES, and NASH (p < 0.05, p < 0.001, p < 0.0001, vs CTRL, one-way ANOVA), while Sod1 and Sod2 mRNA expression was unchanged (Fig. 5a, Supplementary Fig. S7c). Because systemic oxidative stress was observed only in
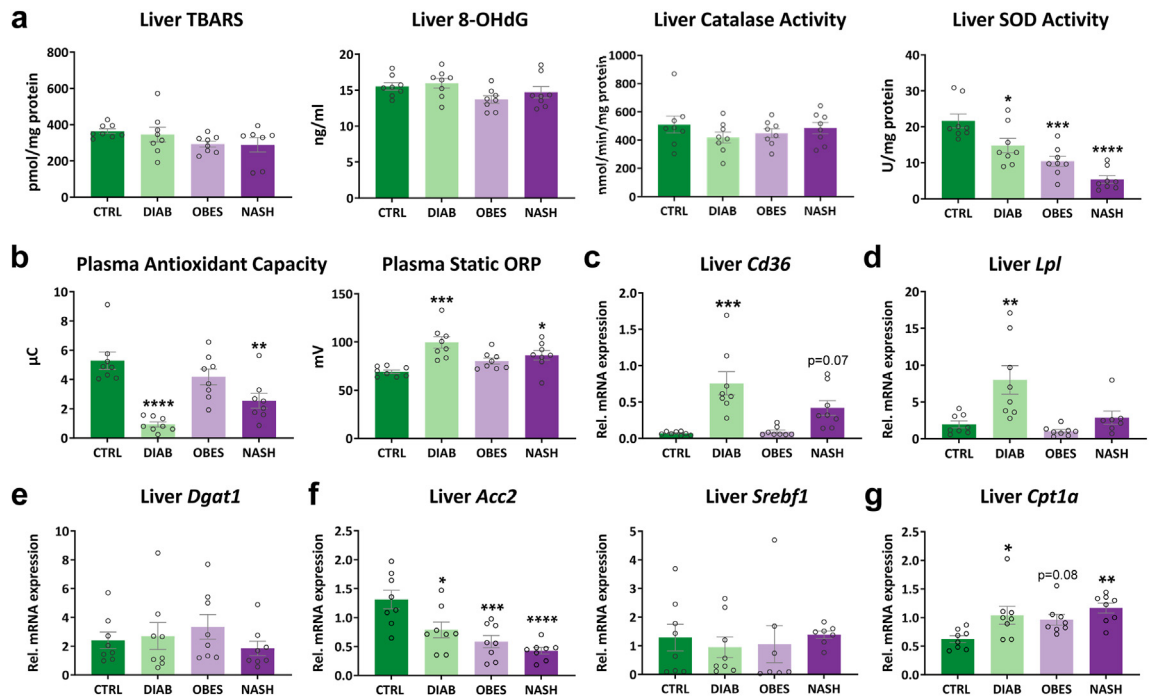
Fig. 5: Alterations of oxidative stress markers and hepatic lipid metabolism (W16). (a) Markers of hepatic oxidative stress. (b) Plasma static oxidation-reduction potential (ORP) and antioxidant capacity as markers for systemic oxidative stress. mRNA level of genes related to (c) lipid uptake, (d) lipolysis, (e) triacylglycerol synthesis, (f) de-novo lipogenesis, and (g) FAO pathways. Mean ± SEM, n = 7–8/group, analysed with 1-way ANOVA. *p < 0.05; **p < 0.01; ***p < 0.001; ****p < 0.0001 vs CTRL. TBARS: thiobarbituric acid reactive substances; 8-OHdG: 8-hydroxy-2′-deoxyguanosine.

hyperglycemic mice, we measured plasma AGE, which revealed comparable levels in all groups (Supplementary Fig. S7d). STZ-induced β cell toxicity is mediated by GLUT2 glucose transporter, we therefore measured TBARS in kidney, which express also GLUT2.[41] There was a trend towards higher TBARS in NASH kidney than in CTRL (p = 0.06, one-way ANOVA) (Supplementary Fig. S7e).

Taken together, systemic, but not hepatic oxidative stress is evident in DIAB and NASH and associates with the higher hepatic mitochondrial respiration.

Liver and adipose tissue lipid metabolism

Hepatic mRNA expression of genes involved in lipid uptake was distinctly altered between the groups, i.e. cluster of differentiation 36 (Cd36) and fatty acid transporter protein 5 (Fatp5) were higher in DIAB, whereas Fabp2 was increased in OBES and NASH compared to CTRL at W16. Also, caveolin1 (Cav1) was increased only in NASH vs CTRL (Fig. 5c, Supplementary Fig. S8a).

Lipid turnover genes e.g. lipoprotein lipase (Lpl) and adipose triglyceride lipase (Atgl) were increased only in DIAB, whereas hormone sensitive lipase (Hsl) and Atgl co-activator, Abhd5, did not change between the groups. Of note, liver Atgl was correlated with overall hepatic

mt-specific $[PMGS]_P$ and $[PMGS]_E$ (Supplementary Fig. S10). In contrast to mRNA data, CD36 and LPL protein level showed similar levels in all groups (Fig. 5d, Supplementary Fig. S8b).

Hepatic mRNA expression of genes involved in tri-acylglycerol synthesis, e.g. diacylglycerol o-acyltransferase (Dgat) 1 and 2, and de-novo lipogenesis (DNL), e.g. sterol regulatory element-binding transcription factor 1 (Srebf1), carbohydrate response element-binding protein (ChREBP), nuclear receptor subfamily 1 group h member 2 (Nr1h2), Nr1h4, and fatty acid synthase 1 (Fasn1, data not shown), and acetyl-CoA carboxylase 1 (Acc1) were not different between the models (Fig. 5e and f, Supplementary Fig. S8c and S8d). Noteworthy, Acc2 was decreased in three groups as compared to CTRL (Fig. 5f) and negatively correlated with overall hepatic mt-specific $[OctM]_P$ and $[OctM]_E$ (r = −0.45, −0.44, respectively, both p < 0.05, correlation t-test). Acc2 is a mitochondrial enzyme responsible for synthesis of malonyl-CoA, a known inhibitor for carnitine palmitoyltransferase I (Cpt1a) activity, a rate limiting enzyme for long chain fatty acid oxidation.[42] Of note, hepatic Cpt1a mRNA was increased in DIAB and NASH and tended to be higher in OBES (p < 0.05, p < 0.01, p = 0.08, respectively vs CTRL, one-way ANOVA) (Fig. 5g). Cpt1a showed also a trend for

positive correlation with overall hepatic mt-specific $[OctM]_P$ and $[OctM]_E$ (r = 0.36, p = 0.06; r = 0.33, p = 0.08, respectively, correlation t-test).

We also assessed genes involved in liver lipid efflux belonging to ATP binding cassette (ABC) superfamily. Only *Abcg1* transporter, which is responsible for cholesterol efflux to HDL,[43] was elevated in NASH and DIAB and correlated with overall hepatic mt-specific $[OctM]_P$ and $[OctM]_E$ (r = 0.44, p = 0.02; r = 0.40, p = 0.03, respectively, correlation t-test), whereas *Abca1* was not different between groups (Supplementary Fig. S8e). Because glucose is a main substrate for DNL,[44] we measured hepatic GLUT2 transporter as well, which showed no difference at mRNA level between the groups, whereas its protein content was decreased in DIAB as compared to CTRL (Supplementary Fig. S8f).

In addition, lipolysis and lipid biosynthesis genes were assessed in EWAT and SWAT. Despite mixed results in lipid synthesis genes, lipolysis genes, *Atgl* and its co-activator, *Abhd5*, were increased in DIAB suggesting increased lipolysis in EWAT. Other lipolysis-related genes such as *Hsl* and *Lpl* did not change between the groups as compared to CTRL (Supplementary Fig. S9a and S9b). On the other hand, OBES and NASH showed reduction in certain lipid synthesis genes such as *Fas1* and *Acc1*, but no alterations in lipolysis-related genes. Interestingly, Patatin-like phospholipase domain-containing protein 3 (*Pnpla3*), which has lipase and transacylase activities and increases the risk of NAFLD and its progression in humans,[45,46] was lower in all groups than in CTRL (Supplementary Fig. S9a and S9b). SWAT showed comparable results to EWAT (Supplementary Fig. S9c and S9d). Of note, lipid lipolysis genes i.e. *Atgl* and *Abhd5* and lipid synthesis, i.e. *Dgat1* in SWAT were positively correlated with overall hepatic mt-specific $[PMGS]_E$ (Supplementary Fig. S10).

In summary, each model shows a distinct hepatic expression profile of lipid metabolism-related genes, with commonly decreased *Acc2* along increased *Cpt1a*, which are both associated with hepatic FAO-derived respiration. Only in DIAB, hepatic and WAT expression of lipolysis-related genes is elevated and associates with hepatic TCA-linked respiration.

Hepatic unfolded protein response

As ER stress represents another pathway possibly contributing to metabolically-driven liver diseases,[47] we further measured biomarkers of the 3 branches of UPR, i.e. PKR-like endoplasmic reticulum kinase (PERK), inositol requiring enzyme 1 (IRE1α), and activating transcription factor (ATF) 6[47] (Fig. 6a). The hepatic PERK downstream target, ATF4, was reduced by 53%, 70%, and 73% in DIAB, OBES, and NASH, respectively (p < 0.05, p < 0.001, p < 0.001, vs CTRL, one-way ANOVA) (Fig. 6b), while CHOP was gradual decreased in OBES and NASH, respectively (p = 0.07; p < 0.01, vs CTRL, one-way ANOVA) (Fig. 6c) and

phosphorylated eukaryotic initiation factor-2α (peIF2α^{S51}) was unchanged (data not shown). Ratios of spliced to total X-box-binding protein 1 (sXBP1/tXBP1) was increased by 58% and 50% in DIAB and NASH (both p < 0.001 vs CTRL, one-way ANOVA), suggesting activation of the IRE1α axis (Fig. 6d). In line, ratios of unspliced XBP1 (uXBP1) to tXBP1 were decreased in both DIAB and NASH (data not shown). Finally, cleaved (active) ATF6, was not different between all groups (Fig. 6e). Interestingly, ER-resident chaperone BiP was decreased by 43–73% in the three models (p < 0.05 in OBES and DIAB, p < 0.001 in NASH vs CTRL, one-way ANOVA) (Fig. 6f).

Most of the altered UPR signaling proteins were correlated with hepatic mt-specific $[OctM]_P$ and $[OctM]_E$, whereas certain UPR proteins (sXBP1, BiP, total IRE1α) were correlated with $[PMGS]_P$ (Fig. 7a and Supplementary Fig. S10). Analysis of these relationships within the different groups showed comparable results (Supplementary Table S1).

Taken together, the three arms of UPR are distinctly altered and associated with hepatic mitochondrial respiration in DIAB, NASH and OBES.

Discussion

This study shows that hepatic, but not soleus muscle mitochondrial oxidation is upregulated during the development of diet-induced obesity and diabetes with or without NASH. Hepatic mitochondrial plasticity, as suggested from the few available human cross-sectional studies,[6,10,48] is operative along with altered tissue-specific insulin sensitivity and lipid metabolism, systemic oxidative stress, and importantly also hepatic ER stress.

The diabetes-related NASH model exhibited the expected course of disease from early steatosis up to evidence for dysplastic hepatocellular nodules.[22,49] This model also showed the highest degree of hypercholesterolemia, probably mediated by increased lipid efflux mechanisms, and impaired hepatic insulin signaling, which likely results from lipotoxic (numerically doubled plasma FFA) and pro-inflammatory mechanisms (increased hepatic TNF-α). While these features resemble some features of human NASH,[50] the reduction in total body weight in line with previous reports[22,49] and the only slightly higher relative fat mass compared to OBES suggest that this NASH model rather represents the phenotype of lean NAFLD[51] or—to certain extent—the novel severe insulin-resistant diabetes endotype (SIRD), which also features higher risk for NAFLD and its progression.[18] Moreover, the higher degree of insulinopenia in both NASH and DIAB compared to the obese mouse model or human T2DM[52,53] represents another specific feature, which will lower insulin-mediated suppression of adipose tissue lipolysis, thereby favoring FFA redistribution and
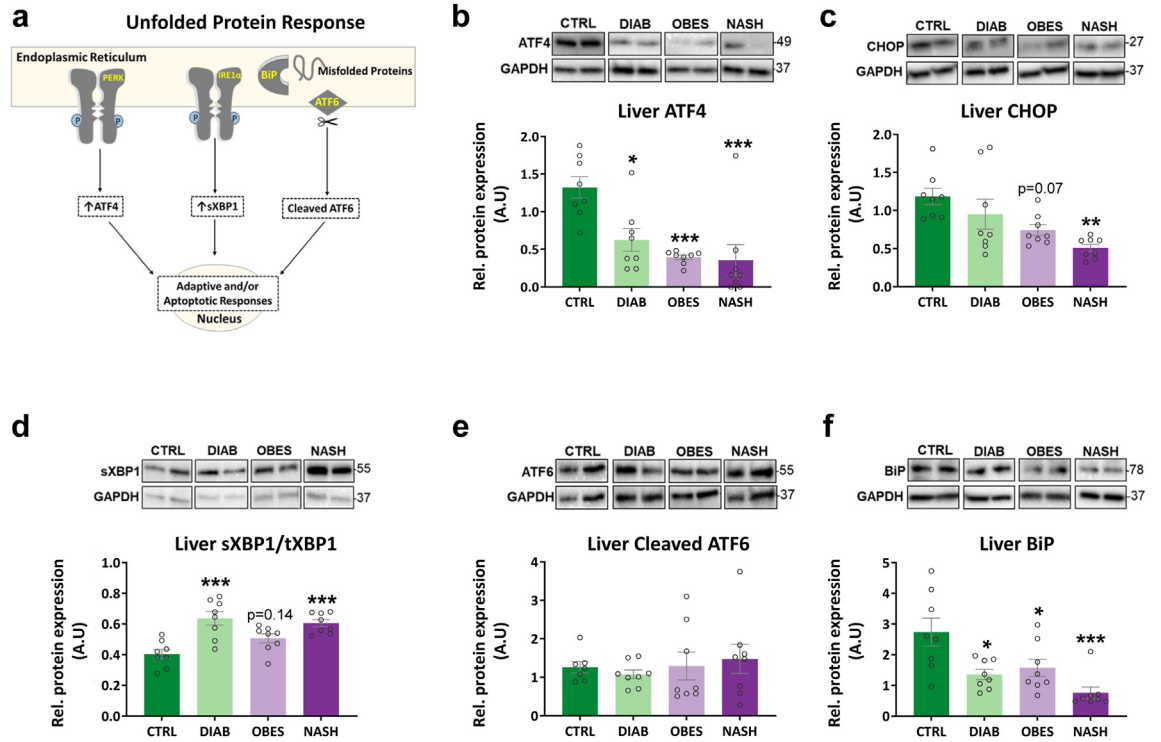
Fig. 6: **Distinctive alterations of markers for endoplasmic reticulum stress (W16).** (a) Cartoon illustrates the canonical unfolded protein response (UPR). (b–f) Immunoblot for markers of UPR accompanied with semi-quantification. Two representative mice were shown for each group based on densitometric quantification. Mean ± SEM, n = 7–8/group, analysed with 1-way ANOVA. *p < 0.05; **p < 0.01; ***p < 0.001 vs CTRL. Total X-box-binding protein 1 (tXBP1) was calculated by summation of spliced (sXBP1) and unspliced (uXBP1) protein level.
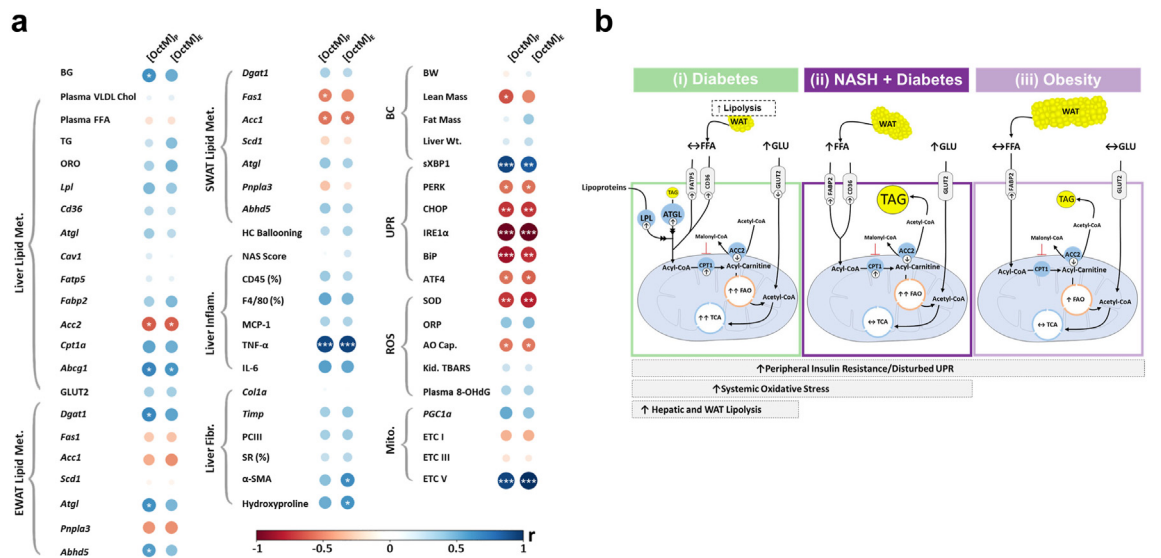

Fig. 7: **Mitochondrial respiratory changes and potential mechanisms.** (a) Correlation plot between different parameters and mt-specific FAO-driven respiration (W16). Size and color of the circles are based on correlation coefficient (r). (b) Cartoon summarizes the main metabolic and respiratory changes and possible mechanisms. Increased FAO respiration was associated with UPR dysfunction, altered hepatic lipid metabolism, and increased systemic oxidative stress and whole-body insulin resistance. Elevated TCA respiration in diabetes is associated with increased liver and white adipose tissue (WAT) lipolysis. BG: blood glucose; Kid. TBARS: kidney thiobarbituric acid reactive substances; BC: body composition; GLU: glucose. *p < 0.05; **p < 0.01; ***p < 0.001 (correlation t-test).

hepatic insulin resistance.[54] This metabolic situation rather resembles the severe insulin-deficient diabetes endotype (SIDD), which has however a lower risk of NAFLD during the early course of diabetes.[18] While these findings further support the notion that the NASH model cannot resemble common NASH,[55] but maybe reflects NAFLD related to certain novel diabetes endotypes.

The NASH model displayed moderate elevation in hepatic coupled FAO-related mitochondrial respiration at W8, which increased further at W16. Hepatic FAO-related respiration was found to be increased also in human NAFLD[10] and NASH without fibrosis,[16] but not in another obese NASH.[13] However, in contrast to FAO, hepatic TCA-related respiration already trended to be lower at W8 and did not differ from CTRL at W16, suggesting an early abnormality of mitochondrial oxidative capacity. Indeed, despite excessive substrate availability, hepatic TCA-linked respiration is not increased in humans with NASH and T2DM than in lean persons[16] or even reduced in humans with severe NASH than in steatotic individuals.[10] This data underline the presence of distinct hepatic mitochondrial abnormalities related to substrates of either lipid or carbohydrate oxidation, which may help to explain the different findings in the few clinical studies.[10,11,13,16,17]

The obese model (OBES) featured insulin resistance, but only slightly higher hepatic FAO-driven respiration and steatosis at W16, suggesting an at least partly sufficient compensation for the prolonged exposure to HFD.[56] Other murine models of diet-induced obesity show more marked increases in hepatic OXPHOS capacity along with insulin resistance,[56–58] which might be due to differences in caloric loads, dietary composition, or even to the applied placebo in these very young mice. Surprisingly, the increase in hepatic FAO-driven respiration was preceded by a transient reduction in uncoupled TCA- and FAO-linked mitochondrial respiration at W8, which is similar to findings in obese-prone rats.[59] The contention of sufficient mitochondrial adaptation in OBES, is supported by the low degree of hepatic steatosis.

In STZ-injected diabetic mice (DIAB), hepatic TCA- and FAO-driven respiration was unchanged at W8, but markedly elevated at W16. This is likely due to chronic insulinopenia leading to hyperglycemia and lipolysis with excessive substrate supply to the liver. Also, high-dose STZ-induced diabetes increased hepatic mitochondrial biogenesis in mice.[60] The relevance of diabetes duration for hepatic mitochondrial function is further supported by elevation of uncoupled mitochondrial respiration after 3 weeks, but not after 9 weeks in STZ-treated male Wistar rats.[61] Other insulinopenic mouse models also showed improved capacity for substrate oxidation[57] or at least transient increase in hepatic OXPHOS capacity.[24] Interestingly, DIAB did not display the expected plasma FFA elevation, which may not only result from to insulinopenia-induced hepatic lipid oxidation,[57] but also from simultaneously increased lipid uptake as demonstrated by higher hepatic *Cd36 and Fatp5* expression. Hepatic *Cd36* not only plays a role in fatty acid uptake, but also in apoptosis, phagocytosis and inflammation.[62] Of note, *Fatp5* is exclusively expressed in liver[63] and elevated in metabolic liver diseases.[64] DIAB featured also higher expression of *Lpl* and *Atgl* in hepatic and adipose tissue reflecting lipid turnover. Although generally low expressed in liver, *Lpl* can be induced by pro-inflammatory cytokines favoring the shunting of circulating triacylglycerol to the liver.[65,66] Higher *Atgl* expression may be due to insulin deficiency,[67] favoring provision of substrates for mitochondrial oxidation to cover the increased metabolic demand of unrestricted gluconeogenesis in DIAB.[57] Insulin deficiency could also account for reduced *Pnpla3* expression in WAT as shown previously.[67] In DIAB, reduced *Pnpla3* could enhance adipose tissue lipolysis by making *Abhd5* available for *Atgl* binding.[68] DIAB showed also lower hepatic GLUT2 expression without change in *Glut2* mRNA level, which may be explained by the observation that GLUT2 protein is a target for STZ at least in murine pancreatic islets.[69] In line with mouse data, DNA chip analysis revealed higher expression of genes involved not only in OXPHOS and glucose, but also lipid metabolism in livers of obese T2DM.[70] While data on hepatic mitochondrial respiration are scarce in human T1DM, the prospective German Diabetes Study (GDS) provided evidence for changing hepatic energy metabolism during the first 5 years after diagnosis of T1DM, occurring independently of liver lipid content.[21]

In contrast to liver, soleus muscle of the three models did not consistently adapt to the various metabolic challenges, similar to reports for NOD mice, as an autoimmune model of T1DM, or transgenic NAFLD models,[24,39] further underlining the tissue-specific differences in mitochondrial adaptation. In line, mitochondrial respiration and ETC protein expression is also reduced in soleus muscle of STZ-induced hypoinsulinemic mice.[71] Also, humans with T1DM and T2DM show impaired skeletal muscle energy metabolism.[6] Of note, the present study employed soleus muscle because of its high mitochondrial content and oxidative capacity[72] and its response to metabolic alterations such as short-term HFD feeding.[73] Although this suggests that other skeletal muscles might be even less responsive in our models, the findings cannot be generalized to other muscles with different fiber type composition.

The mechanisms linking hepatic mitochondrial adaptation to metabolic alterations comprise changes in (i) mitochondrial mass and biogenesis, (ii) lipid metabolism, (iii) insulin sensitivity, (iv) hepatic injury, (v) oxidative stress, and/or (vi) ER stress. First, except for complex V neither other ETC complexes nor expression

of mitochondrial biogenesis-related genes were increased or related to respiration among all mouse models. This reflects results from most obese NASH,[10,13,16] while significant reduction in these parameters was seen mainly in NAFLD with F2–F4 fibrosis.[13] This indicates a decline of mitochondrial biogenesis only in higher fibrosis stages, which was not present in the models of this study. Beyond mitochondrial biogenesis and ETC protein expression, mitochondria are highly dynamic organelles so that it cannot by excluded that the adaptation also involves other mechanisms such as fission, fusion, posttranslational modification or structural organization of ETC and other mitochondrial protein, as discussed previously.[74,75]

Second, this study demonstrated reduced hepatic mitochondrial $Acc2$, which is responsible for the conversion of acetyl-coA to malonyl-CoA that acts as inhibitor for CPT1A, the key enzyme in FAO.[42] Decreased $Acc2$ combined with increased $Cpt1a$ does not only represent a plausible mechanism for the observed increase in FAO, but also provides an explanation for the opposite findings in NASH individuals, who showed decreased hepatic mitochondrial respiration. Those NASH individuals showed not only no difference in CPT1A protein and mRNA, but also reduced activity of the β-hydroxyacyl-CoA dehydrogenase, which is rate limiting enzyme for FAO.[13]

Third, there is an ongoing debate on a causal relationship between mitochondrial function and insulin resistance.[76] The present study confirmed insulin resistance in all models at the level of whole-body,[77,78] but only gradually in liver. While this would argue against a relevant role of hepatic insulin resistance, the rather high clamp insulin dose, which was chosen to provide for identical normoglycemia in these models with different fasting insulinemia, might have masked possible differences in hepatic insulin sensitivity, which have been reported for obese T2DM.[70] Nevertheless, whole-body (skeletal muscle and adipose tissue) insulin resistance may be more relevant for hepatic energy metabolism, e.g. increased lipid flux to the liver.[21] Furthermore, hypoinsulinemia per se could contribute to the higher hepatic respiratory function in NASH and DIAB as shown in severely hyperglycemic and hypoinsulinemic mice.[57] Indeed, prolonged exposure of mouse primary hepatocytes to insulin resulted in reduction in mitochondrial DNA, ATP production and several mitochondrial biogenesis-related genes.[60]

Fourth, this study found no correlation between liver injury markers and mitochondrial respiration, in line with a recent study in obese humans with NAFLD.[17] Nevertheless, the pro-inflammatory cytokine, TNF-α, was positively correlated with maximal coupled FAO- and TCA-linked respiration. Thus, TNF-α might serve as a relevant biomarker of inflammation in metabolic liver diseases, which is further supported by its direct inhibitory effect on mitochondrial respiration of rat hepatocytes[79] and mouse neuronal cells.[80] Another marker of liver injury, α-SMA protein, was positively correlated with TCA-linked respiration. α-SMA reliably reflects activation of hepatic stellate cells, which is involved in would healing and liver fibrosis.[81] As stellate cells show aerobic glycolysis with higher levels of glycolytic enzymes,[82] they might generate TCA substrates supporting hepatocyte mitochondrial respiration in NAFLD.

Fifth, elevated oxidative metabolism has been also linked to greater ROS production and impaired antioxidative defense in progressing NAFLD.[10,40,83] In obese T2DM, OXPHOS gene expression was positively correlated with expression of genes involved in ROS generation and scavenging, e.g. cytochrome $P450$, glutathione-S-transferase and catalase.[70] Surprisingly, measures of circulating, but not hepatic oxidative stress were increased in DIAB and NASH models. This could be due to efficient hepatic mitochondrial coupling and antioxidant defense. Interestingly, the activity but not mRNA expression of SOD, which catalyzes superoxide anion conversion to H_2O_2, was decreased in all three models, possibly hinting at the earliest abnormality of antioxidant defense at this stage of NAFLD. Increased systemic oxidative stress could result from excessive lipolysis and/or hyperglycemia, e.g. via AGE.[84] The absence of changes in total AGE between groups does not exclude differences in specific AGE, which were not measured in the present study. Of note, differential increases of plasma 8-OHdG and kidney TBARS in DIAB and NASH suggest the operation of multiple mechanisms in systemic oxidative stress.

Interestingly, this study observed differential hepatic changes of the three canonical sensors of UPR suggesting homeostatic dysfunction of this pathway due to chronic ER stress.[85] Various common metabolic diseases including NAFLD exhibit ER stress.[47] Other studies showed also selective activation of specific arms of UPR based on the type, dosage and duration of ER stressor.[85,86] For example, IRE1α and PERK arms responded faster to Ca^{2+} release from ER than ATF6,[87] whereas ATF6 was selectively activated in the context of membrane protein expression.[86] Another ER-resident chaperone, BiP, was reduced in the three models, but predominately in NASH, which can favor NALFD progression according to a liver-specific BiP knockout model.[88] Considering the tight contact between ER and mitochondria and the correlation between UPR markers and mitochondrial respiration, one might speculate that a potential organelle cross-talk could contribute to NALFD progression.[89] In support, BiP translocates to mitochondria in ER-stressed cells[90] and BiP accumulated in the hepatic mitochondrial fraction of the DIAB and NASH in the present study (data not shown).

This study aimed at comprehensive examination of representative models of metabolic liver diseases, but certain limitations need to be acknowledged. First,

rodent models of diabetes or NAFLD incompletely reflect the respective human diseases. Since the diabetogenic effect of STZ is dose-dependent,[91] high-dose STZ generally induces severe insulinopenic hyperglycemia, thereby rather reflecting human T1DM or the novel SIDD.[92] Of note, low-dose STZ combined with high fat diets generally creates relative insulinopenia along with insulin resistance and moderate hyperglycemia[93] to resemble human T2DM or the SIRD subtype.[18] Likewise, rodent models incompletely cover the spectrum of human NAFLD.[94] Second, *in vivo* insulin sensitivity was measured with gold-standard methodology, the high-insulin dose HEC, which precisely measures whole-body insulin resistance, but may miss small changes in hepatic insulin resistance. However, assessment of insulin signaling at lower insulin concentrations made it possible to detect differences at the molecular level of the liver. Third, mRNA and protein expression of enzymes were used for assessing lipid metabolism, which does not necessarily reflect *in vivo* metabolic fluxes. Finally, experimental constraints (ethical consideration for *in vivo* animal studies, limited amount of tissue specimen) required to focus on the main outcome, i.e. hepatic mitochondrial respiration, and address only certain other exploratory outcomes. Thus, insulin signaling was assessed specifically in liver, but not in soleus muscle or adipose tissue and molecular mechanisms were investigated mainly at W16, when the most marked alterations in hepatic mitochondrial respiration were recorded. Further, lack of data on mitochondrial ROS production limits the evaluation of liver oxidative balance.

In conclusion, the tested mouse models of diet-induced obesity, insulinopenic diabetes and diabetes-related NAFLD feature distinct upregulation of hepatic FAO-driven respiration in the face of comparable whole-body insulin resistance. The mitochondrial and metabolic adaptations are linked to hepatic UPR dysfunction, systemic oxidative stress, and altered hepatic lipid metabolism. Presence of diabetes further results in higher hepatic TCA-driven respiration, which associated with increased hepatic and adipose tissue lipolysis (Fig. 7b).

Contributors
BD and MR drafted the manuscript; BD, CE, DP, and MR designed experiments; BD, LM, CE, CR, CG, ER, GH, MW, IE, MDF, FZ, and AY performed experiments, collected data, and analyzed the data. MR initiated the study and obtained funding for the study. All authors discussed the results, commented on the manuscript, read and approved the final version of the manuscript. Both BD and MR verified the underlying data of this manuscript.

Data sharing statement
All data presented in this manuscript are available from the corresponding author upon request.

Declaration of interests
LM, CE, CR, CG, ER, DP, MW, IE, MDF, FZ, and AY declare no competing interests. BD is supported by a DZD grant. GH is supported

Appendix A. Supplementary data
Supplementary data related to this article can be found at https://doi.org/10.1016/j.ebiom.2023.104714.

References
1 Chalasani N, Younossi Z, Lavine JE, et al. The diagnosis and management of nonalcoholic fatty liver disease: practice guidance from the American Association for the study of liver diseases. *Hepatology*. 2018;67:328–357.
2 European Association for the Study of the Liver (EASL). European Association for the study of diabetes (EASD), European Association for the study of obesity (EASO). EASL-EASD-EASO clinical practice guidelines for the management of non-alcoholic fatty liver disease. *J Hepatol*. 2016;64:1388–1402.
3 Dewidar B, Kahl S, Pafili K, Roden M. Metabolic liver disease in diabetes - from mechanisms to clinical trials. *Metabolism*. 2020;111S:154299.
4 Gastaldelli A, Cusi K. From NASH to diabetes and from diabetes to NASH: mechanisms and treatment options. *JHEP Rep*. 2019;1:312–328.
5 Mansouri A, Gattolliat C-H, Asselah T. Mitochondrial dysfunction and signaling in chronic liver diseases. *Gastroenterology*. 2018;155:629–647.
6 Koliaki C, Roden M. Alterations of mitochondrial function and insulin sensitivity in human obesity and diabetes mellitus. *Annu Rev Nutr*. 2016;36:337–367.
7 Fromenty B, Roden M. Mitochondrial alterations in fatty liver diseases. *J Hepatol*. 2022;78(2):415–429.
8 Sunny NE, Parks EJ, Browning JD, Burgess SC. Excessive hepatic mitochondrial TCA cycle and gluconeogenesis in humans with nonalcoholic fatty liver disease. *Cell Metab*. 2011;14:804–810.
9 Petersen KF, Befroy DE, Dufour S, Rothman DL, Shulman GI. Assessment of hepatic mitochondrial oxidation and pyruvate cycling in NAFLD by (13)C magnetic resonance spectroscopy. *Cell Metab*. 2016;24:167–171.
10 Koliaki C, Szendroedi J, Kaul K, et al. Adaptation of hepatic mitochondrial function in humans with non-alcoholic fatty liver is lost in steatohepatitis. *Cell Metab*. 2015;21:739–746.
11 Lund MT, Kristensen M, Hansen M, et al. Hepatic mitochondrial oxidative phosphorylation is normal in obese patients with and without type 2 diabetes. *J Physiol*. 2016;594:4351–4358.
12 Pérez-Carreras M, Del Hoyo P, Martín MA, et al. Defective hepatic mitochondrial respiratory chain in patients with nonalcoholic steatohepatitis. *Hepatology*. 2003;38:999–1007.
13 Moore MP, Cunningham RP, Meers GM, et al. Compromised hepatic mitochondrial fatty acid oxidation and reduced markers of mitochondrial turnover in human NAFLD. *Hepatology*. 2022;76(5):1452–1465. https://doi.org/10.1002/hep.32324.
14 Cortez-Pinto H, Chatham J, Chacko VP, Arnold C, Rashid A, Diehl AM. Alterations in liver ATP homeostasis in human nonalcoholic steatohepatitis: a pilot study. *JAMA*. 1999;282:1659–1664.

15 Sanyal AJ, Campbell-Sargent C, Mirshahi F, et al. Nonalcoholic steatohepatitis: association of insulin resistance and mitochondrial abnormalities. *Gastroenterology.* 2001;120:1183–1192.

16 Gancheva S, Kahl S, Pesta D, et al. Impaired hepatic mitochondrial capacity in nonalcoholic steatohepatitis associated with type 2 diabetes. *Diabetes Care.* 2022;45(4):928–937.

17 Pedersen JS, Rygg MO, Chrøis K, et al. Influence of NAFLD and bariatric surgery on hepatic and adipose tissue mitochondrial biogenesis and respiration. *Nat Commun.* 2022;13:2931.

18 Zaharia OP, Strassburger K, Strom A, et al. Risk of diabetes-associated diseases in subgroups of patients with recent-onset diabetes: a 5-year follow-up study. *Lancet Diabetes Endocrinol.* 2019;7:684–694.

19 Wolf P, Fellinger P, Pfleger L, et al. Reduced hepatocellular lipid accumulation and energy metabolism in patients with long standing type 1 diabetes mellitus. *Sci Rep.* 2019;9:2576.

20 Gancheva S, Bierwagen A, Kaul K, et al. Variants in genes controlling oxidative metabolism contribute to lower hepatic ATP independent of liver fat content in type 1 diabetes. *Diabetes.* 2016;65:1849–1857.

21 Kupriyanova Y, Zaharia OP, Bobrov P, et al. Early changes in hepatic energy metabolism and lipid content in recent-onset type 1 and 2 diabetes mellitus. *J Hepatol.* 2021;74:1028–1037.

22 Fujii M, Shibazaki Y, Wakamatsu K, et al. A murine model for non-alcoholic steatohepatitis showing evidence of association between diabetes and hepatocellular carcinoma. *Med Mol Morphol.* 2013;46:141–152.

23 Pesta D, Gnaiger E. High-resolution respirometry: OXPHOS protocols for human cells and permeabilized fibers from small biopsies of human muscle. *Methods Mol Biol.* 2012;810:25–58.

24 Jelenik T, Séquaris G, Kaul K, et al. Tissue-specific differences in the development of insulin resistance in a mouse model for type 1 diabetes. *Diabetes.* 2014;63:3856–3867.

25 Hernández EÁ, Kahl S, Seelig A, et al. Acute dietary fat intake initiates alterations in energy metabolism and insulin resistance. *J Clin Invest.* 2017;127:695–708.

26 Steele R. Influences of glucose loading and of injected insulin on hepatic glucose output. *Ann N Y Acad Sci.* 1959;82:420–430.

27 Finegood DT, Bergman RN, Vranic M. Modeling error and apparent isotope discrimination confound estimation of endogenous glucose production during euglycemic glucose clamps. *Diabetes.* 1988;37:1025–1034.

28 Kuang J, Saner NJ, Botella J, et al. *Methodological considerations when assessing mitochondrial respiration and biomarkers for mitochondrial content in human skeletal muscle.* 2021.

29 Larsen S, Nielsen J, Hansen CN, et al. Biomarkers of mitochondrial content in skeletal muscle of healthy young human subjects. *J Physiol.* 2012;590:3349–3360.

30 Bobe G, Cobb TJ, Leonard SW, et al. Increased static and decreased capacity oxidation-reduction potentials in plasma are predictive of metabolic syndrome. *Redox Biol.* 2017;12:121–128.

31 Lefkowitch JH. Special stains in diagnostic liver pathology. *Semin Diagn Pathol.* 2006;23:190–198.

32 Kleiner DE, Brunt EM, Van Natta M, et al. Design and validation of a histological scoring system for nonalcoholic fatty liver disease. *Hepatology.* 2005;41:1313–1321.

33 Lattouf R, Younes R, Lutomski D, et al. Picrosirius red staining: a useful tool to appraise collagen networks in normal and pathological tissues. *J Histochem Cytochem.* 2014;62:751–758.

34 Mehlem A, Hagberg CE, Muhl L, Eriksson U, Falkevall A. Imaging of neutral lipids by oil red O for analyzing the metabolic status in health and disease. *Nat Protoc.* 2013;8:1149–1154.

35 Jensen EC. Quantitative analysis of histological staining and fluorescence using ImageJ. *Anat Rec.* 2013;296:378–381.

36 Bankhead P, Loughrey MB, Fernández JA, et al. QuPath: open source software for digital pathology image analysis. *Sci Rep.* 2017;7:16878.

37 Hartwig V, Dewidar B, Lin T, et al. Human skin-derived ABCB5+ stem cell injection improves liver disease parameters in Mdr2KO mice. *Arch Toxicol.* 2019;93:2645–2660.

38 Livak KJ, Schmittgen TD. Analysis of relative gene expression data using real-time quantitative PCR and the 2(-Delta Delta C(T)) method. *Methods.* 2001;25:402–408.

39 Jelenik T, Kaul K, Séquaris G, et al. Mechanisms of insulin resistance in primary and secondary nonalcoholic fatty liver. *Diabetes.* 2017;66:2241–2253.

40 Satapati S, Kucejova B, Duarte JAG, et al. Mitochondrial metabolism mediates oxidative stress and inflammation in fatty liver. *J Clin Invest.* 2015;125:4447–4462.

41 Nahdi AMTA, John A, Raza H. Elucidation of molecular mechanisms of streptozotocin-induced oxidative stress, apoptosis, and mitochondrial dysfunction in Rin-5F pancreatic β-cells. *Oxid Med Cell Longev.* 2017;2017:7054272.

42 Strable MS, Ntambi JM. Genetic control of de novo lipogenesis: role in diet-induced obesity. *Crit Rev Biochem Mol Biol.* 2010;45:199–214.

43 Kennedy MA, Barrera GC, Nakamura K, et al. ABCG1 has a critical role in mediating cholesterol efflux to HDL and preventing cellular lipid accumulation. *Cell Metab.* 2005;1:121–131.

44 Sanders FWB, Griffin JL. De novo lipogenesis in the liver in health and disease: more than just a shunting yard for glucose. *Biol Rev Camb Philos Soc.* 2016;91:452–468.

45 Sookoian S, Pirola CJ. PNPLA3, the triacylglycerol synthesis/hydrolysis/storage dilemma, and nonalcoholic fatty liver disease. *World J Gastroenterol.* 2012;18:6018–6026.

46 Zaharia OP, Strassburger K, Knebel B, et al. Role of patatin-like phospholipase domain-containing 3 gene for hepatic lipid content and insulin resistance in diabetes. *Diabetes Care.* 2020;43:2161–2168.

47 Lebeaupin C, Vallée D, Hazari Y, Hetz C, Chevet E, Bailly-Maître B. Endoplasmic reticulum stress signalling and the pathogenesis of non-alcoholic fatty liver disease. *J Hepatol.* 2018;69:927–947.

48 Szendroedi J, Phielix E, Roden M. The role of mitochondria in insulin resistance and type 2 diabetes mellitus. *Nat Rev Endocrinol.* 2011;8:92–103.

49 Saito T, Muramatsu M, Ishii Y, et al. Pathophysiological analysis of the progression of hepatic lesions in STAM mice. *Physiol Res.* 2017;66:791–799.

50 Targher G, Lonardo A, Byrne CD. Nonalcoholic fatty liver disease and chronic vascular complications of diabetes mellitus. *Nat Rev Endocrinol.* 2018;14:99–114.

51 VanWagner LB, Armstrong MJ. Lean NAFLD: a not so benign condition? *Hepatol Commun.* 2018;2:5–8.

52 Targher G, Corey KE, Byrne CD, Roden M. The complex link between NAFLD and type 2 diabetes mellitus - mechanisms and treatments. *Nat Rev Gastroenterol Hepatol.* 2021;18:599–612.

53 Pafili K, Roden M. Nonalcoholic fatty liver disease (NAFLD) from pathogenesis to treatment concepts in humans. *Mol Metab.* 2021;50:101122.

54 Roden M, Shulman GI. The integrative biology of type 2 diabetes. *Nature.* 2019;576:51–60.

55 Farrell G, Schattenberg JM, Leclercq I, et al. Mouse models of nonalcoholic steatohepatitis: toward optimization of their relevance to human nonalcoholic steatohepatitis. *Hepatology.* 2019;69:2241–2257.

56 Begriche K, Massart J, Robin M-A, Bonnet F, Fromenty B. Mitochondrial adaptations and dysfunctions in nonalcoholic fatty liver disease. *Hepatology.* 2013;58:1497–1507.

57 Franko A, von Kleist-Retzow J-C, Neschen S, et al. Liver adapts mitochondrial function to insulin resistant and diabetic states in mice. *J Hepatol.* 2014;60:816–823.

58 Crescenzo R, Bianco F, Falcone I, Coppola P, Liverini G, Iossa S. Increased hepatic de novo lipogenesis and mitochondrial efficiency in a model of obesity induced by diets rich in fructose. *Eur J Nutr.* 2013;52:537–545.

59 Morris EM, Jackman MR, Meers GME, et al. Reduced hepatic mitochondrial respiration following acute high-fat diet is prevented by PGC-1α overexpression. *Am J Physiol Gastrointest Liver Physiol.* 2013;305:G868–G880.

60 Liu H-Y, Yehuda-Shnaidman E, Hong T, et al. Prolonged exposure to insulin suppresses mitochondrial production in primary hepatocytes. *J Biol Chem.* 2009;284:14087–14095.

61 Ferreira FM, Palmeira CM, Seiça R, Moreno AJ, Santos MS. Diabetes and mitochondrial bioenergetics: alterations with age. *J Biochem Mol Toxicol.* 2003;17:214–222.

62 Rada P, González-Rodríguez Á, García-Monzón C, Valverde ÁM. Understanding lipotoxicity in NAFLD pathogenesis: is CD36 a key driver? *Cell Death Dis.* 2020;11:1–15.

63 Anderson CM, Stahl A. SLC27 fatty acid transport proteins. *Mol Aspect Med.* 2013;34:516.

64 Enooku K, Tsutsumi T, Kondo M, et al. Hepatic FATP5 expression is associated with histological progression and loss of hepatic fat in NAFLD patients. *J Gastroenterol.* 2020;55:227–243.

65 Merkel M, Weinstock PH, Chajek-Shaul T, et al. Lipoprotein lipase expression exclusively in liver. A mouse model for metabolism in the neonatal period and during cachexia. *J Clin Invest*. 1998;102:893–901.

66 Wilson CG, Tran JL, Erion DM, Vera NB, Febbraio M, Weiss EJ. Hepatocyte-specific disruption of CD36 attenuates fatty liver and improves insulin sensitivity in HFD-fed mice. *Endocrinology*. 2016;157:570–585.

67 Kershaw EE, Hamm JK, Verhagen LAW, Peroni O, Katic M, Flier JS. Adipose triglyceride lipase: function, regulation by insulin, and comparison with adiponutrin. *Diabetes*. 2006;55:148–157.

68 Yang A, Mottillo EP, Mladenovic-Lucas L, Zhou L, Granneman JG. Dynamic interactions of ABHD5 with PNPLA3 regulate triacylglycerol metabolism in brown adipocytes. *Nat Metab*. 2019;1:560–569.

69 Gai W, Schott-Ohly P, Schulte im Walde S, Gleichmann H. Differential target molecules for toxicity induced by streptozotocin and alloxan in pancreatic islets of mice in vitro. *Exp Clin Endocrinol Diabetes*. 2004;112:29–37.

70 Takamura T, Misu H, Matsuzawa-Nagata N, et al. Obesity upregulates genes involved in oxidative phosphorylation in livers of diabetic patients. *Obesity*. 2008;16:2601–2609.

71 Franko A, von Kleist-Retzow JC, Böse M, et al. Complete failure of insulin-transmitted signaling, but not obesity-induced insulin resistance, impairs respiratory chain function in muscle. *J Mol Med*. 2012;90:1145–1160.

72 Varikmaa M, Bagur R, Kaambre T, et al. Role of mitochondria-cytoskeleton interactions in respiration regulation and mitochondrial organization in striated muscles. *Biochim Biophys Acta*. 2014;1837:232–245.

73 Morales PE, Monsalves-Álvarez M, Tadinada SM, et al. Skeletal muscle type-specific mitochondrial adaptation to high-fat diet relies on differential autophagy modulation. *FASEB J*. 2021;35:e21933.

74 Legaki A-I, Moustakas II, Sikorska M, Papadopoulos G, Velliou R-I, Chatzigeorgiou A. Hepatocyte mitochondrial dynamics and bioenergetics in obesity-related non-alcoholic fatty liver disease. *Curr Obes Rep*. 2022;11:126–143.

75 Mathers KE, Staples JF. Differential posttranslational modification of mitochondrial enzymes corresponds with metabolic suppression during hibernation. *Am J Physiol Regul Integr Comp Physiol*. 2019;317:R262–R269.

76 Sergi D, Naumovski N, Heilbronn LK, et al. Mitochondrial (Dys) function and insulin resistance: from pathophysiological molecular mechanisms to the impact of diet. *Front Physiol*. 2019;10:532.

77 Rosso C, Mezzabotta L, Gaggini M, et al. Peripheral insulin resistance predicts liver damage in nondiabetic subjects with nonalcoholic fatty liver disease. *Hepatology*. 2016;63:107–116.

78 Gaggini M, Morelli M, Buzzigoli E, DeFronzo RA, Bugianesi E, Gastaldelli A. Non-alcoholic fatty liver disease (NAFLD) and its connection with insulin resistance, dyslipidemia, atherosclerosis and coronary heart disease. *Nutrients*. 2013;5:1544–1560.

79 Stadler J, Bentz BG, Harbrecht BG, et al. Tumor necrosis factor alpha inhibits hepatocyte mitochondrial respiration. *Ann Surg*. 1992;216:539–546.

80 Doll DN, Rellick SL, Barr TL, Ren X, Simpkins JW. Rapid mitochondrial dysfunction mediates TNF-alpha-induced neurotoxicity. *J Neurochem*. 2015;132:443–451.

81 Friedman SL. Hepatic stellate cells: protean, multifunctional, and enigmatic cells of the liver. *Physiol Rev*. 2008;88:125–172.

82 Hou W, Syn W-K. Role of metabolism in hepatic stellate cell activation and fibrogenesis. *Front Cell Dev Biol*. 2018;6:150.

83 Pessayre D, Fromenty B. NASH: a mitochondrial disease. *J Hepatol*. 2005;42:928–940.

84 Bansal S, Siddarth M, Chawla D, Banerjee BD, Madhu SV, Tripathi AK. Advanced glycation end products enhance reactive oxygen and nitrogen species generation in neutrophils in vitro. *Mol Cell Biochem*. 2012;361:289–296.

85 Gomez JA, Rutkowski DT. Experimental reconstitution of chronic ER stress in the liver reveals feedback suppression of BiP mRNA expression. *Elife*. 2016;5:e20390.

86 Maiuolo J, Bulotta S, Verderio C, Benfante R, Borgese N. Selective activation of the transcription factor ATF6 mediates endoplasmic reticulum proliferation triggered by a membrane protein. *Proc Natl Acad Sci U S A*. 2011;108:7832–7837.

87 DuRose JB, Tam AB, Niwa M. Intrinsic capacities of molecular sensors of the unfolded protein response to sense alternate forms of endoplasmic reticulum stress. *Mol Biol Cell*. 2006;17:3095–3107.

88 Ji C, Kaplowitz N, Lau MY, Kao E, Petrovic LM, Lee AS. Liver-specific loss of GRP78 perturbs the global unfolded protein response and exacerbates a spectrum of acute and chronic liver diseases. *Hepatology*. 2011;54:229–239.

89 López-Crisosto C, Bravo-Sagua R, Rodriguez-Peña M, et al. ER-to-mitochondria miscommunication and metabolic diseases. *Biochim Biophys Acta*. 2015;1852:2096–2105.

90 Sun F-C, Wei S, Li C-W, Chang Y-S, Chao C-C, Lai Y-K. Localization of GRP78 to mitochondria under the unfolded protein response. *Biochem J*. 2006;396:31–39.

91 Junod A, Lambert AE, Stauffacher W, Renold AE. Diabetogenic action of streptozotocin: relationship of dose to metabolic response. *J Clin Invest*. 1969;48:2129–2139.

92 Herder C, Roden M. A novel diabetes typology: towards precision diabetology from pathogenesis to treatment. *Diabetologia*. 2022;65:1770–1781.

93 Srinivasan K, Viswanad B, Asrat L, Kaul CL, Ramarao P. Combination of high-fat diet-fed and low-dose streptozotocin-treated rat: a model for type 2 diabetes and pharmacological screening. *Pharmacol Res*. 2005;52:313–320.

94 Gallage S, Avila JEB, Ramadori P, et al. A researcher's guide to preclinical mouse NASH models. *Nat Metab*. 2022;4:1632–1649.